JOURNAL

OF THE AMERICAN CHEMICAL SOCIETY

VOLUME 106, NUMBER 26 DECEMBER 26, 1984

Quantum Chemical Studies of a Model for Peptide Bond Formation. 3. Role of Magnesium Cation in Formation of Amide and Water from Ammonia and Glycine

Tetsuro Oie,[†] Gilda H. Loew,*[†] Stanley K. Burt,[‡] and Robert D. MacElroy[§]

Contribution from the The Rockefeller University, Molecular Theory Laboratory, Palo Alto, California 94304, Molecular Research Institute, Palo Alto, California 94304, and NASA-Ames Research Center, Extraterrestrial Biology Division, Moffett Field, California 94035.
Received October 28, 1983

Abstract: The S_N2 reaction between glycine and ammonia molecules with magnesium cation Mg^{2+} as a catalyst has been studied as a model reaction for Mg^{2+}-catalyzed peptide bond formation using the ab initio Hartree–Fock molecular orbital method. As in previous studies of the uncatalyzed and amine-catalyzed reactions between glycine and ammonia, two reaction mechanisms have been examined, i.e., a two-step and a concerted reaction. The stationary points of each reaction including intermediate and transition states have been identified and free energies calculated for all geometry-optimized reaction species to determine the thermodynamics and kinetics of each reaction. Substantial decreases in free energies of activation were found for both reaction mechanisms in the Mg^{2+}-catalyzed amide bond formation compared with those in the uncatalyzed and amine-catalyzed amide bond formation. The catalytic effect of the Mg^{2+} cation is to stabilize both the transition states and intermediate, and it is attributed to the neutralization of the developing negative charge on the electrophile and formation of a conformationally flexible nonplanar five-membered chelate ring structure.

Introduction

The origin of life most probably occurred as part of a sequence of chemical processes driven by energy sources available in the environment of the primitive earth, and constrained by the physical condition of that environment. One of the major objectives in origin of life studies is to identify the significant events in the evolution of protein synthesis, from nondirected amino sequences, dependent on the intrinsic factors such as monomer concentration, energy availability, and the intrinsic stereochemistry of the forming polymers, to extrinsically directed (templated) amino acid sequences.

In approaching this objective, there have been numerous attempts to synthesize polypeptides from their component amino acids under conditions that resemble those of the primitive earth. The information thus obtained has been used to postulate the environmental requirements for the formation of prebiotic proteins. Attempts[1] have been made to activate amino acids by a variety of methods including esterification, phosphorylation, and the presence of divalent cations (e.g., Mg^{2+}, Ca^{2+}, Cu^{2+}, Ni^{2+}, etc.). Such activation is required, since none of the free amino acid forms, whether cationic, zwitterionic, or anionic, present in solution at any pH are viable candidates for peptide bond formation because of the presence of a protonated amino or anionic carboxylate group.[2] However, the design of effective experiments and the interpretation of results have been hampered by a lack of detailed information about the mechanism of peptide formation. Therefore, we have undertaken systematic studies of this mechanism under a variety of conditions using the techniques of theoretical chemistry. Theoretical studies by quantum mechanical methods can provide valuable and detailed information about reaction mechanisms, that is, the nature of transition states and transient intermediates, which cannot be readily characterized by experimental techniques.

As a first step in understanding the mechanism of peptide bond formation, we have reported in previous papers[3] a thorough in-

[†] The Rockefeller University.
[‡] Molecular Research Institute.
[§] NASA-Ames Research Center.

(1) (a) Weber, A. L.; Orgel, L. E. *J. Mol. Evol.* **1981**, *17*, 190. (b) Lahav, N.; White, D. H. *Ibid.* **1980**, *16*, 11. (c) Weber, A. L.; Orgel, L. E. *Ibid.* **1980**, *16*, 1. (d) Mullins, D. W.; Lacey, J. C. *Ibid.* **1980**, *15*, 339. (e) Weber, A. L.; Orgel, L. E. *Ibid.* **1979**, *13*, 185. (f) Weber, A. L.; Orgel, L. E. *Ibid.* **1978**, *11*, 189. (g) Weber, A. L.; Orgel, L. E. *Ibid.* **1978**, *11*, 9. (h) Steinman, G.; Cole, M. N. *Proc. Natl. Acad. Sci. U.S.A.* **1967**, *58*, 735. (i) Steinman, G. *Arch. Biochem. Biophys.* **1967**, *121*, 533. (j) Steinman, G.; Kenyon, D. H.; Calvin, M. *Biochim. Biophys. Acta* **1966**, *124*, 339. (k) Ponnamperuma, C.; Peterson, E. *Science* **1965**, *147*, 1572. (l) Steinman, G.; Kenyon, D. H.; Calvin, M. *Nature (London)* **1965**, *206*, 707. (m) Steinman, G.; Lemmon, R. M.; Calvin, M. *Proc. Natl. Acad. Sci. U.S.A.* **1964**, *52*, 27. (n) Yamada, S.; Wagatsuma, M.; Takeuchi, Y.; Terashima, S. *Chem. Pharm. Bull.* **1971**, *19*, 2380. (o) Yamada, S.; Terashima, S.; Wagatsuma, M. *Tetrahedron Lett.* **1970**, 1501. (p) Buckingham, D. A.; Foster, D. M.; *Sargeson*, A. M. *J. Am. Chem. Soc.* **1970**, *92*, 5701. (q) Buckingham, D. A.; Deckers, J.; Sargeson, A. M. *Ibid.* **1973**, *95*, 4173.

(2) Hay, R. W.; Porter, L. J. *J. Chem. Soc.* **1967**, 1261.

(3) (a) Oie, T.; Loew, G. H.; Burt, S. K.; Binkley, J. S.; MacElroy, R. D. *J. Am. Chem. Soc.* **1982**, *104*, 6169. (b) Oie, T.; Loew, G. H.; Burt, S. K.; MacElroy, R. D. *Ibid.* **1983**, *105*, 2221. (c) Oie, T.; Loew, G. H.; Burt, S. K.; Binkley, J. S.; MacElroy, R. D. *Int. J. Quantum Chem.; Quantum Biol. Symp.* **1982**, *9*, 223. (d) Oie, T.; Loew, G. H.; Burt, S. K.; MacElroy, R. D. *J. Comput. Chem.* **1983**, *4*, 449.

0002-7863/84/1506-8007$01.50/0

vestigation of the process of amide bond formation between formic acid and ammonia and between glycine and ammonia with and without amine catalysis:

$$NH_3 + HCOOH \rightarrow HCONH_2 + H_2O \quad (1a)$$

$$NH_3 + NH_2CH_2COOH \rightarrow NH_2CH_2CONH_2 + H_2O \quad (1b)$$

$$NH_3 + HCOOH + NH_3 \rightarrow HCONH_2 + H_2O + NH_3 \quad (2a)$$

$$NH_3 + NH_2CH_2COOH + NH_3 \rightarrow NH_2CH_2CONH_2 + H_2O + NH_3 \quad (2b)$$

using ab initio molecular orbital methods. These reactions (1a–2b) involving neutral acids should closely correspond to peptide bond formation between two amino acid esters. Esterification enhances peptide bond formation most likely by transforming amino acids to neutral species, which makes a nucleophilic attack of the amino nitrogen on an electrophilic carbonyl carbon more feasible than for zwitterionic or anionic amino acids themselves. In reactions 2a and 2b, the second ammonia molecule is assumed to act as a catalyst. Kinetic studies[4] of aminolysis reaction of aliphatic esters with primary and secondary amines have revealed a rate law containing a term, predominantly second order in amine, at moderate and high concentration of amine. This result indicates that such reactions are susceptible to amine catalysis by a second amine molecule. Similarly, peptide bond formation could also be amine catalyzed by a second molecule of an amino acid ester. To further investigate this possibility, free energies of activation were calculated for reactions 2a and 2b and compared with those for 1a and 1b. These results clearly demonstrated that a second ammonia molecule does catalyze amide bond formation. Two reaction mechanisms were examined, a two-step reaction via an intermediate and a concerted reaction. These were found to be fairly competitive for the uncatalyzed reactions (1a and 1b), while for the catalyzed reactions (2a and 2b), the two-step mechanism is more favorable than the concerted one. Although aminolysis of esters is generally believed to proceed through a tetrahedral intermediate, such an intermediate has never been isolated. The results obtained provide additional evidence for a two-step reaction which indeed proceeds through a tetrahedral intermediate found to be energetically fairly unstable.

A fairly large free energy of activation calculated for these model reactions indicates that activation of amino acids by esterification alone or together with amine catalysis is not efficient enough to lead to the facile formation of a peptide bond. This result is consistent with the very low yield (4% at best) of diglycine obtained either in aqueous[1f] or nonaqueous[1o] solution by condensation reactions of glycine ethyl esters.

However, in the presence of metal cations such as Cu^{2+}, Mg^{2+}, and Co^{3+}, formation of dipeptide is greatly enhanced both in aqueous and nonaqueous solutions. The yield of diglycine for the condensation of glycine ethyl esters is about 20 and 40% in the presence of Mg^{2+} and Cu^{2+} cations, respectively, in anhydrous ethanol solution[1n] and is over 50% in the presence of Co^{3+} cation in aqueous solution.[1p]

Another advantage of the presence of metal cations is that they prevent formation of diketopiperazine (DKP) which occurs to a greater extent than diglycine formation in the absence of metal cations. The formation of DKP occurs by an internal cyclization of dipeptide and is an obstacle to further elongation of dipeptides.

Thus, given the abundance of metal cations in the primitive earth, it is very likely that they played a significant role in the formation of prebiotic peptides.

Therefore, we report here the results of studies of the role of magnesium dication in the amide bond formation between ammonia and glycine molecules using the ab initio molecular orbital method.

The catalytic effect of metal cations on peptide bond formation and the high yield are believed to arise from direct activation of

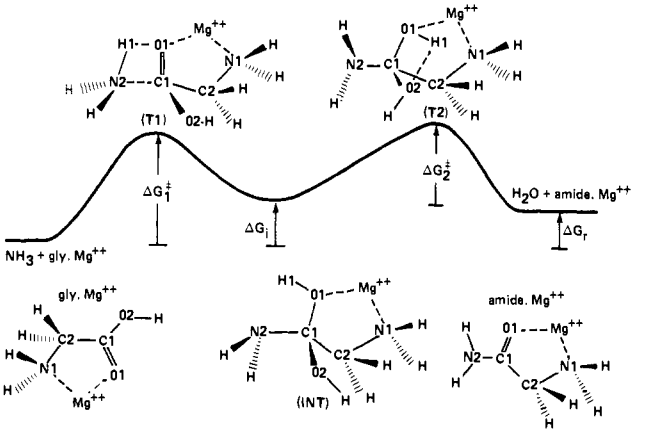

Figure 1. Two-step reaction mechaism for the Mg^{2+}-catalyzed ammonia–glycine reaction and the free energy diagram of the reaction.

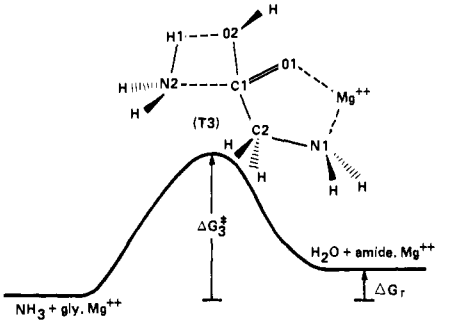

Figure 2. Concerted mechanism for the Mg^{2+}-catalyzed ammonia–glycine reaction and the free energy diagram of the reaction.

the carbonyl group via chelation with its oxygen atom and the amino nitrogen atom from synthetic studies using various metal dications[1n-q] and mechanistic study using Co^{3+} ion[1p,q] for the formation of diglycine. Although formation of an intermediate from such chelated complexes was detected spectrophotometrically during peptide synthesis from the condensation reaction between a Co^{3+} isopropylglycinate chelate and glycine ethyl ester,[1q] such an intermediate has never been isolated. Moreover, nothing is known about the nature and energy of the transition states. Such information is essential to characterize and to understand the details of the role of metal cations in peptide bond formation. The reaction studied:

$$NH_3 + NH_2CH_2COOH \cdot Mg^{2+} \rightarrow NH_2CH_2CONH_2 \cdot Mg^{2+} + H_2O \quad (3)$$

should closely correspond to peptide bond formation between two amino acids esters. The anionic form of α-amino acids is known to form a five-membered planar chelate ring with metal cations by X-ray diffraction studies.[5] Infrared studies in solution indicate that the ester of α-amino acids could also form the same chelate complex with a metal cation.[1n] Thus, we consider Mg^{2+}-coordinated glycine (see Figure 1) rather than uncoordinated glycine as a reactant.

As in the previous studies of uncatalyzed and NH_3-catalyzed amide bond formations, we have examined two possible mechanisms for Mg^{2+}-catalyzed amide bond formation: a two-step reaction (Figure 1) and a concerted reaction (Figure 2).

In the two-step mechanism the reactions is assumed to take place through a stable or metastable intermediate (INT). The first step, reactant to intermediate, represents C–N bond formation through a nucleophilic attack of the nitrogen atom on a carbonyl carbon atom. In the second step, intermediate to product, a water

(4) (a) Bunnett, J. F.; Davis, G. T. *J. Am. Chem. Soc.* **1960**, *82*, 665. (b) Jencks, W. P.; Carriuolo, J. *Ibid.* **1960**, *82*, 675. (c) Blackburn, G. M.; Jencks, W. P. *Ibid.* **1968**, *90*, 2638.

(5) (a) Freeman, H. C.; Snow, M. R.; Nitta, I.; Tomita, K. *Acta Crystallogr.* **1964**, *17*, 1463. (b) Freeman, H. C. *Adv. Protein Chem.* **1967**, *22*, 257.

molecule is released by C–O and O–H bond cleavages.

In the concerted mechanism of this reaction, both C–N bond formation and release of a water molecule by N–H and C–O bond cleavages take place simultaneously. In contrast to the first mechanism, in which a hydrogen atom is transferred to the carbonyl oxygen from ammonia, the concerted mechanism involves transfer of a hydrogen to the hydroxyl oxygen atom.

Method and Results

To characterize these two reaction mechanisms, ab initio molecular orbital calculations were carried out using the GAUSSIAN 80 program.[6] Analytical gradient optimization methods were used to locate the minima, corresponding to reactant, intermediate, and product, and saddle points, corresponding to transition states using an STO-3G basis set,[7] where all the geometrical parameters were optimized (convergence of the root mean square of gradients is 0.001 hartree/bohr or radian).

To locate the stationary points (especially saddle points) on this reaction energy surface, it is absolutely necessary to have fairly accurate initial geometries and matrices of second derivatives of the energy (i.e., Hessian matrix). To obtain these initial values, the following approach was taken. First, a two-dimensional potential energy surface was calculated using an STO-2G basis set.[7] In this procedure, two appropriate degrees of freedom representing formation and cleavage of the bond were chosen as independent variables (i.e., H1–O1 and N2–C1 bond lengths for the first transition state, and H1–O2 and C1–O2 bond lengths for the second transition state of the two-step reaction, and H1–O2 and C1–N2 bond lengths of the concerted reaction), and all the remaining degrees of freedom were optimized. The results were used to help identify a probable reaction pathway, and also to locate possible transition states and intermediates on the energy surface. The geometries of candidate transition states and intermediates obtained by this procedure were used as initial geometries and for the calculation of initial Hessian matrix required for the total geometry optimization of intermediate and transition states using an STO-3G basis set.

All the transition states thus found were further verified by calculation of force constants to determine the presence of one negative eigenvalue of the force constant matrix (i.e., the matrix of the second partial derivaties of the potential energy). The requirement that the force constant matrix has one negative eigenvalue to define a transition state is a physical consequence of the loss of one degree of vibrational freedom at the transition state, i.e., $3N - 7$ vibrational modes, in contrast to the energy minima which have $3N - 6$ eigenvalues, which are all positive, where N is the number of atoms in a molecule.

For all stationary points found using an STO-3G basis set, the harmonic vibrational frequencies and normal coordinates were determined by solving for eigenvalues and eigenvectors of the mass-weighted Cartesian force constant matrix, $\mathbf{M}^{-1/2}\mathbf{F}\mathbf{M}^{-1/2}$, where $\mathbf{M}$ is a diagonal matrix of atomic masses and $\mathbf{F}$ is a Cartesian force constant matrix.[8] The eigenvector corresponding to a negative eigenvalue of this matrix for each transition state (T1, T2, and T3), is the reaction coordinate for each reaction. These are shown in Figure 3 as a set of normalized mass-weighted Cartesian displacement vectors $\mathbf{M}^{1/2}\mathbf{X}$, where $\mathbf{X}$ is the Cartesian displacement vector.

Also shown in Figure 3 is the prospective structure of each of the three transition states and the intermediate obtained using an STO-3G basis set. Corresponding values of optimized geometric parameters for the transition states and the intermediate as well as for the reactant and product are given in Table I, where for comparison the corresponding geometrical parameters for the uncatalyzed NH_3–glycine reaction obtained in the previous study are also given. Reported values for this study represent convergence to 0.003 Å for bond length and 0.3° for bond and dihedral angles.

The STO-3G optimized geometries were then used for single-point Hartree–Fock (HF) calculations with the 6-31G basis

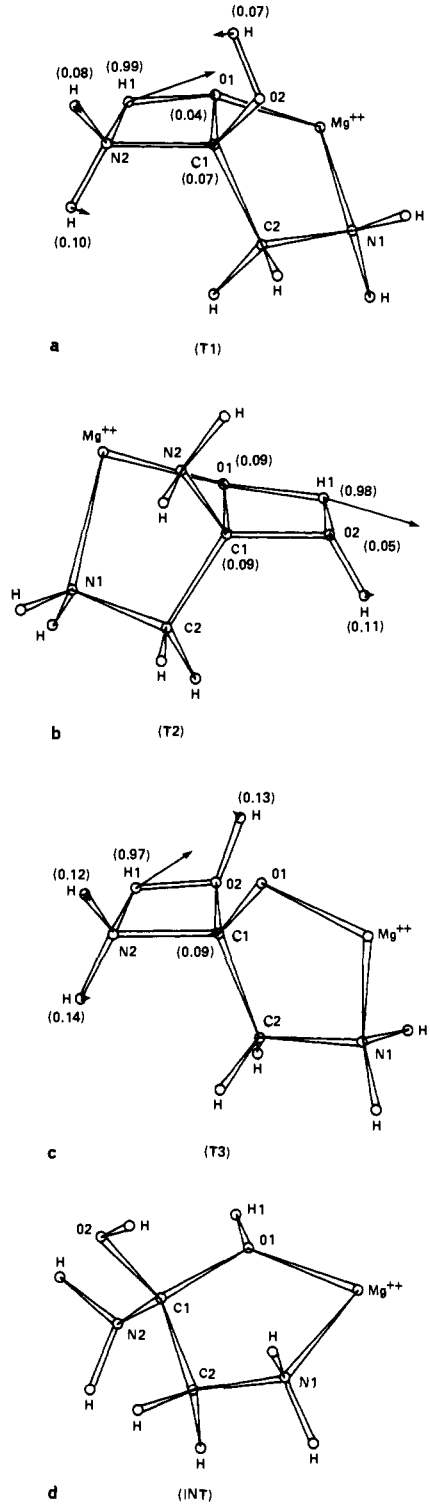

Figure 3. (a) Structure of transition state T1 optimized by STO-3G basis set. The components of the normalized reaction coordinate are shown as mass-weighted Cartesian displacement vectors of each atom with the relative amplitude given in parentheses and the direction shown by the arrow. (b) Structure of transition state T2 optimized by STO-3G basis set. The reaction coordinate is also given. (c) Structure of transition state T3 optimized by STO-3G basis set. The reaction coordinate is also given. (d) Structure of intermediate INT optimized by STO-3G basis set.

(6) Binkley, J. S.; Whiteside, R. A.; Krishnan, R.; Seeger, R.; DeFrees, D. J.; Schlegel, H. B; Topiol, S.; Kahn, L. R.; Pople, J. A. GAUSSIAN 80, QCPE 406, Indiana University.

(7) (a) Hehre, W. J.; Stewart, R. F.; Pople, J. A. *J. Chem. Phys.* **1969**, *51*, 2657. (b) Hehre, W. J.; Ditchfield, R.; Stewart, R. F.; Pople, J. A *Ibid.* **1970**, *52*, 2769.

(8) Wilson, E. B.; Decius, J. C.; Cross, R. C. "Molecular Vibrations"; McGraw-Hill: New York, 1955.

Table I. STO-3G Optimized Structures of Reactant, Product, Intermediate, and Transition States for Mg^{2+}-Catalyzed NH_3–Glycine Reaction[a]

parameter		parameter		parameter		parameter	
	Reactant: $NH_2CH_2COOH{\cdot}Mg^{2+}$				Transition State T1		
C1=O1	1.267 (1.217)	∠O1C1C2	121.1	N2—H1	1.219 (1.132)	∠N1MgO1	93.9
C1—O2	1.320 (1.389)	∠C1C2N1	108.2 (113.6)	N2—C1	1.530 (1.779)	∠MgO1C1	108.4
C1—C2	1.558 (1.552)	∠C2N1Mg	106.3	H1—O1	1.262 (1.385)	∠O1C1C2	111.7
C2—N1	1.517 (1.482)	∠O2C1O1	124.0 (122.4)	C1=O1	1.438 (1.320)	∠C1C2N1	106.3
N1—Mg	1.968	$\tau_{N1MgO1C1}$	0.0	C1—O2	1.402 (1.402)	∠C2N1Mg	103.5
O1—Mg	1.817	$\tau_{MgO1C1C2}$	0.0	C1—C2	1.569 (1.569)	τ_{O2C1O1}	115.3
H—O2	0.995 (0.990)	$\tau_{O1C1C2N1}$	0.0	C2—N1	1.519 (1.484)	$\tau_{H1O1C1N2}$	−0.1 (0.0)
H—C2	1.096 (1.091)	$\tau_{C1C2N1Mg}$	0.0	N1—Mg	1.966	$\tau_{N1MgO1C1}$	11.5
H—N1	1.037 (1.034)	$\tau_{C2N1MgO1}$	0.0	O1—Mg	1.787	$\tau_{MgO1C1C2}$	−33.8
∠N1MgO1	91.4	$\tau_{O2C1C2N1}$	180.0	H—N2	1.037 (1.033)	$\tau_{O1C1C2N1}$	44.8
∠MgO1C1	112.9			H—O2	0.991 (0.990)	$\tau_{C1C2N1Mg}$	−31.9
	Product: $NH_2CH_2CONH_2{\cdot}Mg^{2+}$			∠H1N2C1	76.3 (69.8)	$\tau_{C2N1MgO1}$	13.2
C1=O1	1.281 (1.218)	∠O1–C1–C2	119.9	∠N2C1O1	89.8 (88.8)	$\tau_{O2C1C2N1}$	−82.7 (−171.3)
C1—N2	1.335 (1.440)	∠C1C2N1	108.8 (113.5)	∠C1O1H1	78.6 (80.5)	$\tau_{N2C1C2N1}$	145.7 (74.4)
C1—C2	1.563 (1.556)	∠C2N1Mg	105.8	∠O1H1N2	115.3 (120.9)		
C2—N1	1.517 (1.482)	∠O1C1N2	121.9 (123.3)		Transition State T2		
N1—Mg	1.968	$\tau_{N1MgO1C1}$	−0.8	N2—C1	1.499 (1.445)	∠N1MgO1	90.1
O1—Mg	1.798	$\tau_{MgO1C1C2}$	−0.2	H1—O1	1.452 (1.363)	∠MgO1C1	85.7
H—N2	1.026 (1.027)	$\tau_{O1C1C2N1}$	1.5	H1—O2	1.079 (1.080)	∠O1C1C2	112.8
H—C2	1.095 (1.092)	$\tau_{C1C2N1Mg}$	−1.8	C1—O1	1.408 (1.318)	∠C1C2N1	101.3
H-N1	1.036 (1.034)	$\tau_{C2N1MgO1}$	1.5	C1—O2	1.467 (1.735)	∠C2N1Mg	99.9
∠N1MgO1	91.9	$\tau_{N2C1C2N1}$	−178.7	C1—C2	1.566 (1.571)	∠N2C1O1	103.6 (119.8)
∠Mg–O1–C1	113.5			C2—N1	1.521 (1.483)	$\tau_{H1O1C1O2}$	1.3 (−0.1)
	Intermediate (INT)			N1—Mg	2.012	$\tau_{N1MgO1C1}$	−54.4
N2—C1	1.461 (1.489)	∠O1C1C2	105.6 (111.8)	O1—Mg	1.826	$\tau_{MgO1C1C2}$	73.3
H1—O1	0.982 (0.988)	∠C1C2N1	112.2 (112.8)	H—O2	0.994 (0.990)	$\tau_{O1C1C2N1}$	−53.1
C1—O1	1.493 (1.431)	∠C2N1Mg	105.3	∠O1H1O2	109.0 (120.6)	$\tau_{C1C2N1Mg}$	1.5
C1—O2	1.407 (1.429)	∠O2C1O1	107.9 (106.2)	∠H1O2C1	84.2 (71.7)	$\tau_{C2N1MgO1}$	32.5
C1—C2	1.581 (1.567)	$\tau_{N1MgO1C1}$	−6.8	∠O2C1O1	92.2 (87.2)	$\tau_{O2C1C2N1}$	−161.3 (−77.4)
C2—N1	1.522 (1.483)	$\tau_{MgO1C1C2}$	−10.1	∠C1O1H1	74.5 (80.5)	$\tau_{N2C1C2N1}$	60.6 (167.4)
N1—Mg	1.948	$\tau_{O1C1C2N1}$	28.2		Transition State T3		
O1—Mg	1.801	$\tau_{C1C2N1Mg}$	−32.6	H1—O2	1.158 (1.182)	∠O1C1C2	117.0
∠N2C1O1	104.7 (108.4)	$\tau_{C2N1MgO1}$	22.0	H1—N2	1.314 (1.224)	∠C1C2N1	109.0
∠N1MgO1	89.9	$\tau_{O2C1C2N1}$	−91.6 (−60.8)	N2—C1	1.525 (1.679)	∠C2N1Mg	103.1
∠MgO1C1	117.7	$\tau_{N2C1C2N1}$	141.8 (175.3)	C1—O2	1.506 (1.610)	∠O2C1O1	112.0
				C1=O1	1.355 (1.232)	∠N2C1O1	115.4
				C1—C2	1.584 (1.573)	∠N2C1C2	112.3
				C2—N1	1.515 (1.485)	$\tau_{H1O2C1N2}$	−0.1 (0.7)
				N1—Mg	1.965	$\tau_{N1MgO1C1}$	3.1
				O1—Mg	1.769	$\tau_{MgO1C1C2}$	10.3
				∠H1N2C1	75.4 (73.7)	$\tau_{O1C1C2N1}$	−22.8
				∠N2C1O2	87.7 (81.8)	$\tau_{C1C2N1Mg}$	21.5
				∠C1O2H1	80.7 (77.5)	$\tau_{C2N1MgO1}$	−15.1
				∠O2H1N2	116.2 (127.0)	$\tau_{O2C1C2N1}$	105.1 (85.8)
				∠N1MgO1	94.8	$\tau_{N2C1C2N1}$	−159.6 (171.1)
				∠MgO1C1	111.3		

[a] See Figures 1–3 for the structures. Bond lengths (X—Y or X=Y) in Å; bond angles (∠XYZ) and dihedral angles (τ_{WXYZ}) in degrees, where W, X, Y, and Z refer to atoms as in Figures 1–3. The STO-3G optimized parameters for the uncatalyzed NH_3–NH_2CH_2COOH reaction are given in parenthesis (see ref 3d).

set.[9] The validity of this procedure is based on the assumption that the STO-3G optimized structures will provide a reasonable basis for calculating the relative energies at a higher level of theory. One set of calculations made in the previous studies of NH_3-catalyzed[3b] and uncatalyzed[3a] amide bond formation between the ammonia and formic acid molecules showed that the relative energies calculated with the 3-21G basis set were not significantly affected (0.6–3.5 kcal/mol for the three transition states), when the STO-3G optimized geometries were used instead of the 3-21G optimized structures. This observation was also made by Schlegel and coworkers for their studies of tautomerization energies of formamide, 2-pyridone, and 4-pyridone,[10a], and by Radom and co-workers for their studies of the $C_2H_5O^+$ potential surface.[10b]

In order to obtain the relative Gibbs free energies (G) of the reaction species, entropy (S) terms as well as thermal energy (V) contributions to relative enthalpies were calculated. For these calculations, the STO-3G optimized geometries were used to obtain the translational (tr), rotational (rot), and vibrational (vib) contributions to the relative enthalpies and entropies. The formulas for these entities were derived from the molecular partition function:[11]

$$G(T) = U + V(T) - TS(T)$$

$$V(T) = V_{tr}(T) + V_{rot}(T) + V_{vib}(T)$$

$$S(T) = S_{tr}(T) + S_{rot}(T) + S_{vib}(T)$$

where U is the potential energy (internal energy at 0 K) excluding zero-point vibrational energy, which is included in $V_{vib}(T)$. The detailed formulas of the terms $V(T)$ and $S(T)$ are given in a previous paper.[3c] The relative free energies, entropies, and thermal

(9) (a) Hehre, W. J.; Ditchfield, R.; Pople, J. A. *J. Chem. Phys.* **1972**, *56*, 2257. (b) Francl, M. M.; Pietro, W. J.; Hehre, W. J.; Binkley, J. S.; Gordon, M. S.; DeFrees, D. J.; Pople, J. A. *Ibid.* **1982**, *77*, 3654.

(10) (a) Schlegel, H. B.; Gund, P.; Fluder, E. M. *J. Am. Chem. Soc.* **1982**, *104*, 5347. (b) Nobes, H. R.; Rodwell, R. W.; Bouma, J. W.; Radom, L. *Ibid.* **1981**, *103*, 1913.

(11) Hertzberg, G. "Molecular Spectra and Molecular Structure: II. Infrared and Raman Spectra of Polyatomic Molecules"; Van Nostrand: Toronto, 1968; Chapter 5.

Table II. Ab Initio Calculations on Relative Energies for Mg^{2+}-Catalyzed NH_3–Glycine Reaction and Comparison with NH_3-Catalyzed and Uncatalyzed NH_3–Glycine and NH_3–HCOOH Reactions[a]

	T1	T2	INT	T3	R
			Mg^{2+}-Catalyzed NH_3–Glycine Reaction		
	$\Delta U^{\ddagger}_1$ ($\Delta G^{\ddagger}_1$)	$\Delta U^{\ddagger}_2$ ($\Delta G^{\ddagger}_2$)	ΔU_i (ΔG_i)	$\Delta U^{\ddagger}_3$ ($\Delta G^{\ddagger}_3$)	ΔU_r (ΔG_r)
HF/6-31G//A	3.7 (16.8)	22.7 (23.8)	−9.8 (3.8)	13.6 (26.7)	−28.7 (−29.5)
	$T\Delta S^{\ddagger}_1$	$T\Delta S^{\ddagger}_2$	$T\Delta S_i$	$T\Delta S^{\ddagger}_3$	$T\Delta S_r$
HF/STO-3G//A	−12.6	−2.4	−11.2	12.5	0.0
	$\Delta V^{\ddagger}_1$	$\Delta V^{\ddagger}_2$	ΔV_i	$\Delta V^{\ddagger}_3$	ΔV_r
HF/STO-3G//A	0.5	−1.3	2.4	0.6	−0.8
			Uncatalyzed NH_3–Glycine Reaction		
	$\Delta U^{\ddagger}_1$ ($\Delta G^{\ddagger}_1$)	$\Delta U^{\ddagger}_2$ ($\Delta G^{\ddagger}_2$)	ΔU_i (ΔG_i)	$\Delta U^{\ddagger}_3$ ($\Delta G^{\ddagger}_3$)	ΔU_r (ΔG_r)
HF/6-31G//A	46.4 (57.8)	49.9 (47.0)	1.1 (15.3)	56.6 (68.9)	0.8 (−0.2)
	$T\Delta S^{\ddagger}_1$	$T\Delta S^{\ddagger}_2$	$T\Delta S_i$	$T\Delta S^{\ddagger}_3$	$T\Delta S_r$
HF/STO-3G//A	−12.2	−0.4	−11.7	−12.4	0.0
			NH_3-Catalyzed NH_3–Glycine–NH_3 Reaction		
	$\Delta U^{\ddagger}_1$ ($\Delta G^{\ddagger}_1$)	$\Delta U^{\ddagger}_2$ ($\Delta G^{\ddagger}_2$)	ΔU_i (ΔG_i)	$\Delta U^{\ddagger}_3$ ($\Delta G^{\ddagger}_3$)	ΔU_r (ΔG_r)
HF/6-31G//A	15.9 (42.2)	24.7 (36.7)	1.1 (15.3)	35.9 (62.0)	0.8 (−0.2)
			Uncatalyzed NH_3–HCOOH Reaction[b]		
	$\Delta U^{\ddagger}_1$ ($\Delta G^{\ddagger}_1$)	$\Delta U^{\ddagger}_2$ ($\Delta G^{\ddagger}_2$)	ΔU_i (ΔG_i)	$\Delta U^{\ddagger}_3$ ($\Delta G^{\ddagger}_3$)	ΔU_r (ΔG_r)
MP4/6-31G**//B	41.6 (52.7)	41.8 (38.9)	3.3 (16.4)	46.9 (57.5)	0.4 (0.0)
HF/6-31G//A	42.2 (53.3)	47.8 (44.9)	−0.6 (12.5)	54.6 (65.2)	−1.2 (−1.6)
			NH_3-Catalyzed NH_3–HCOOH–NH_3 Reaction[c]		
	$\Delta U^{\ddagger}_1$ ($\Delta G^{\ddagger}_1$)	$\Delta U^{\ddagger}_2$ ($\Delta G^{\ddagger}_2$)	ΔU_i (ΔG_i)	$\Delta U^{\ddagger}_3$ ($\Delta G^{\ddagger}_3$)	ΔU_r (ΔG_r)
MP2/6-31G**//B	13.8 (38.9)	15.1 (25.8)	3.6 (16.7)	25.0 (50.3)	0.0 (−0.4)
HF/6-31G//A	13.6 (38.7)	21.3 (32.0)	−0.6 (12.5)	33.4 (58.7)	−1.2 (−1.6)

[a] All relative energies, ΔU, ΔG, $T\Delta S$, and ΔV are in kcal/mol. G (free energy), S (entropy), and V (sum of the translational, rotational, and vibrational enthalpies) are calculated at 298.15 K and 1 atm. U is the Hartree–Fock (HF) or Möller–Plesset perturbative energy at the second (MP2) and the fourth (MP4) orders. The fourth-order MP4 calculation includes all single, double, and quadruple substitutions, i.e., MP4(SDQ). All the energies are relative to the energy of reactant except that the energy of T2 is relative to that of INT for reactions 1a, 1b, and 3, and the sum of the energies of INT and NH_3 for reactions 2a and 2b. The energies of the product relative to those of the reactant are given in the last column. Note that $G = U - TS + V$. The method and basis sets used for geometry optimization and single point energy calculation are given at the right and left sides of //, respectively, where A = HF/STO-3G and B = HF/3-21G. [b] See ref 3a. [c] See ref 3b.

energies calculated at 298.15 K and 1 atm are summarized in Table II. For comparison, the energetics obtained in the previous studies of uncatalyzed and NH_3-catalyzed amide bond formations between NH_3 and glycine molecules are also given in Table II.

Discussion

Nature of Transition States and Intermediates. As was found in the uncatalyzed NH_3–glycine reaction (reaction 1b), the results obtained for the Mg^{2+}-catalyzed NH_3–glycine reaction (reaction 3) indicates that Mg^{2+}-catalyzed peptide bond formation does not proceed by a simple nucleophilic attack of an amine nitrogen on a carbonyl carbon atom. Instead, two alternative mechanisms were obtained, each involving complex four-centered interactions between the nitrogen and hydrogen atoms of the amine, and the carboxyl carbon and oxygen atoms of the glycine molecule. No transition state involving only nucleophilic attack of the amine nitrogen on the carbonyl carbon was found. As was found in the uncatalyzed reaction, all the transition states observed here also form planar four-centered rings through this four-centered interaction.

One of these mechanisms, involving the carbonyl oxygen, is a two-step reaction in which N–C bond formation via transition state T1 leads to an intermediate (INT). The second step then involves elimination of H_2O from this intermediate via the second transition state (T2). The other mechanism involves the hydroxyl oxygen and leads in one step to amide with loss of H_2O via transition state T3.

Every stationary point of both reaction pathways contained a five-membered Mg^{2+} cation chelate ring. This ring is planar for the reactant and product, and nonplanar for the intermediate and all the transition states. Thus, all the transition states are characterized by a planar four-membered and a nonplanar five-membered bicyclic ring structure, and are hence more complex and more difficult to identify than those found in the uncatalyzed reaction.

In Figure 3 the reaction coordinate obtained using an STO-3G basis set is shown, with normalized mass-weighted Cartesian displacement vectors of each atom as its components. These reaction coordinates clearly show that T1 leads to formation of the intermediate, while T2 and T3 lead to formation of the product. As was found in the uncatalyzed NH_3–glycine reaction, the largest and major component is a displacement vector of a transferring hydrogen atom in the four-membered ring.

As is shown in Table I, comparison of the transition states for the Mg^{2+}-catalyzed and uncatalyzed reactions shows that the location of a transferring hydrogen atom in the four-membered ring is comparable in both reactions: at T1 the partially formed O1–H1 bond is longer than the partially broken N2–H1 bond, i.e., 1.262 vs. 1.219 Å and 1.385 vs. 1.132 Å, for the catalyzed and uncatalyzed reactions, respectively; at T2 the partially formed O2–H1 bond is much shorter than the partially broken O1–H1 bond, i.e., 1.079 vs. 1.452 Å and 1.080 vs. 1.363 Å, for the catalyzed and uncatalyzed reactions, respectively; at T3 the partially formed O2–H1 bond is shorter than the partially broken H1–N2 bond, i.e., 1.158 vs. 1.314 Å and 1.182 vs. 1.224 Å for the catalyzed and uncatalyzed reactions, respectively.

As is seen in Figure 3, the displacement vector of the transferring H1 atom is directed toward the lone pair of the target oxygen atom, i.e., the O1 atom for T1 and T3, and the O2 atom for T3. The direction of this vector is not significantly changed by the presence of a Mg^{2+} cation as indicated by a comparison of bond angles ∠C1–O1–H1 (78.6 vs. 80.5°) at T1, ∠C1–O1–H1 (74.5 vs. 80.5°) at T2, and ∠C1–O2–H1 (80.7 vs. 77.5°) for the uncatalyzed and catalyzed reactions.

In each transition state in the catalyzed reactions, the carbonyl C1=O1 bond is longer than the corresponding one in the uncatalyzed reaction due to the O1···Mg^{2+} interaction. Further, the extent of this elongation in the transition states relative to the reactant is enhanced in the catalyzed reaction compared to the uncatalyzed reaction. The greater elongation of the C1=O1 bond

facilitates the transformation of the rigid planar five-membered chelate ring formed by the reactant to a flexible nonplanar five-membered ring in the transition states leading to a lower energy of activation.

Substantially decreased bond lengths of the formed C1–N2 bonds at T1 and T3 are observed in the Mg^{2+}-catalyzed reaction compared with those in the uncatalyzed reaction, i.e., 1.530 vs. 1.779 Å at T1 and 1.525 vs. 1.679 Å at T3. This more complete bond formation is attributable mainly to an increased electrophilicity of the carbonyl carbon atom C1 (net charge increase from 0.30 to 0.42) due to chelation of Mg^{2+} with a carbonyl oxygen atom of the glycine molecule.

In previous studies of the uncatalyzed NH_3–glycine reaction, it was found that about 0.2 electron was transferred from ammonia to glycine at transition states T1 and T3. Most of this electron density is tranferred to the carbonyl oxygen atom O1. In the Mg^{2+}-catalyzed reaction, there is more electron transfer, about 0.5 electron, from the ammonia to the glycine molecule in these transition states, but it is more delocalized. Specifically, the net negative charge on the O1 atom is about the same in the uncatalyzed and catalyzed reaction. Thus, the presence of the Mg^{2+} cation has two effects: it helps to neutralize the developing negative charge on the carbonyl oxygen in transition states T1 and T3 and enhances charge transfer from nucleophilic to electrophilic molecules. This enhanced charge transfer is also associated with a closer contact (shorter C1–N2 bond) between the two reactant molecules in these transition states. Electron transfer to the O1 atom contributes to the stability of the transition states by enhancing the electrostatic interaction with the Mg^{2+} cation. This enhancement is reflected in a shorter distance between the O1 atom and Mg^{2+} cation than the corresponding distance in the reactant or product molecule, 1.787 Å at T1 and 1.769 Å at T3.

The tetrahedral intermediate (INT) in which Mg^{2+} forms a nonplanar, five-membered chelate ring (see Figure 3) is also found in the Mg^{2+}-catalyzed reaction. Despite the presence of this ring, the remaining geometric features of the intermediates formed in the uncatalyzed and catalyzed reactions are similar. Mg^{2+} catalysis leads to much smaller changes in bond lengths and angles (around C1) in the INT than in the transition states. Thus, the conformational flexibility of the ring in the intermediate as well as the interaction of the Mg^{2+} cation with N1 and O1 atoms enhances the stability of the (INT) in the catalyzed reaction.

Transition state T2 is much closer to the intermediate; i.e., the reaction leading to the formation of product is less advanced in the catalyzed than in the uncatalyzed reaction. This difference is illustrated in the length of the partially broken C1–O2 bond, 1.467 and 1.735 Å in the catalyzed vs. uncatalyzed reactions compared to their bond lengths in the INT 1.407 and 1.429 Å.

It is interesting to note that despite their bicyclic structures, all the transition states obtained in the Mg^{2+}-catalyzed reaction are less rigid than those found in the uncatalyzed reaction. This flexibility is indicated by the smaller calculated values of the imaginary frequencies, 1524*i*, 1090*i*, and 1282*i* cm^{-1} for T1, T2, and T3, respectively, compared with those in the uncatalyzed reaction, where the corresponding values are 1780*i*, 1673*i*, and 1379*i* cm^{-1}.

Energetics. In Table II, the energetics obtained at the HF/6-31G level for the three different systems are given, i.e., uncatalyzed, NH_3-catalyzed, and Mg^{2+}-catalyzed amide bond formations between ammonia and glycine molecules.

This table summarizes the internal energies ΔU, the entropies ΔS, the thermal energies ΔV, and the Gibbs free energies ΔG for all the stationary points of the two reaction pathways of the Mg^{2+}-catalyzed reaction. For comparison, the corresponding values of ΔU and ΔG obtained in the previous studies of amide bond formation (i.e., reactions 1a, 1b, 2a, and 2b) are also given in Table II. All the energies given in Table II are relative to the energy of the reactant, except that the energies of the second transition state (T2) in the two-step reaction are given relative to those of the intermediate for the reactions 1a, 1b, and 3, and to the sum of the energies of the intermediate (INT) and catalyst NH_3 for NH_3-catalyzed reactions 2a and 2b. Throughout the following discussion all energy comparisons refer to free energy, unless otherwise noted.

A comparison of the Mg^{2+}-catalyzed reaction with the uncatalyzed reaction shows fairly large decreases in all free energies ΔG by Mg^{2+}, i.e., 41.0, 24.0 (34.7), 11.5, 42.2, and 29.3 kcal/mol for $\Delta G^{\ddagger}_1$, $\Delta G^{\ddagger}_2$ ($\Delta G^{\ddagger}_2 + \Delta G_i$), ΔG_i, $\Delta G^{\ddagger}_3$, and ΔG_r, respectively. Further, the large decrease in ΔG is due mainly to large decreases in the internal energies ΔU, i.e., 42.7, 27.2 (24.0), 10.9, 43.0, and 29.5 kcal/mol for $\Delta U^{\ddagger}_1$, $\Delta U^{\ddagger}_2$ ($\Delta U^{\ddagger}_2 + \Delta U_i$), ΔU_i, $\Delta U^{\ddagger}_3$, and ΔU_r, respectively, since the contributions from entropies ΔS and thermal energy ΔV to the free energies ΔG are nearly the same in the catalyzed and uncatalyzed reactions.

Compared even with the NH_3-catalyzed reaction, the much lower free energies of activation in the Mg^{2+}-catalyzed reaction indicate that the metal cation is indeed a highly efficient catalyst in the formation of a peptide bond between amino acid esters.

In the uncatalyzed NH_3–glycine reaction, it was found that all the transition states were more polar than the reactant, product, and intermediate, and that significant charge separation occurs owing to electron transfer from the incoming NH_3 to glycine at T1 and T3, and from the leaving H_2O to the forming amide at T2. Thus, the large decrease in free energies of activation observed in the Mg^{2+}-catalyzed reaction is understandable. The vacant valence orbitals of Mg^{2+} can accomodate the electrons transferred and hence stabilize the highly polar transition states in a manner similar to solvent molecule stabilization of polar solute molecules.

The intermediate (INT) found in the Mg^{2+}-catalyzed reaction is much more stable than that found in the uncatalyzed reaction (i.e., 3.8 vs. 15.3 kcal/mol for ΔG_i). This calculated enhanced stability is consistent with the spectrophotometrical detection of the intermediate reported in Co^{3+}-catalyzed peptide bond formation.

The substantial decrease in the free energy of reaction (ΔG_r) in the Mg^{2+}-catalyzed reaction is due most probably to the enhanced contribution of ionic forms of the amide bond stabilized by the Mg^{2+} cation, i.e., $N—C{=}O\cdots Mg^{2+} \leftrightarrow N^{+}{=}C—O^{-}\cdots Mg^{2+}$. This enhanced polarization is also reflected in the increase in positive net charge on the amide hydrogen in the presence of Mg^{2+}, i.e., +0.30 vs. +0.18. This enhancement is consistent with the experimental finding that the amide proton of a dipeptide is made more acidic by coordination of a metal cation to the amide carbonyl oxygen.

The relative order of free energies of activation $\Delta G^{\ddagger}$ in the Mg^{2+}-catalyzed reaction is found to be different from that in the uncatalyzed reaction. In the uncatalyzed two-step reaction, the formation of intermediate is slower than the decomposition of it, i.e., $\Delta G^{\ddagger}_1$ (57.8 kcal/mol) > $\Delta G^{\ddagger}_2$ (47.0 kcal/mol), while in the catalyzed reaction the reverse is found, i.e., $\Delta G^{\ddagger}_1$ (16.8 kcal/mol) < $\Delta G^{\ddagger}_2$ (23.8 kcal/mol). On the other hand, relative to the reactant, the activation energy of the second step is slightly higher than that of the first step, i.e., $\Delta G^{\ddagger}_2 + \Delta G_i > \Delta G^{\ddagger}_1$ in both catalyzed (27.6 vs. 23.8 kcal/mol) and uncatalyzed (62.3 vs. 57.8 kcal/mol) reactions. Under both conditions then the overall rate of reaction by this mechanism is affected by both steps.

In the Mg^{2+}-catalyzed reaction, the two-step and concerted mechanisms are found to be equally competitive as is seen by comparing $\Delta G^{\ddagger}_3$ (26.7 kcal/mol) with $\Delta G^{\ddagger}_2 + \Delta G_i$ (27.6 kcal/mol).

In the present and previous studies of model amide bond formation (i.e., reactions 3, 1a, and 1b), the reactions were assumed to take place in an aprotic and hydrophobic environment. However, in protic solution, a more complex reaction mechanism is expected, whether the mechanism is stepwise or concerted. Specifically, solvent molecules with dual proton-donor and -acceptor capability, such as water and ammonia molecules, could be directly involved in the transition states. In fact, our previous studies of NH_3-catalyzed NH_3–HCOOH and NH_3–glycine reactions (2a and 2b) demonstrated this involvement. These studies showed that in both the two-step and concerted mechanisms, a catalytic NH_3 molecule acts both as a proton acceptor from the nucleophilic NH_3 molecule and as a proton donor to the electrophilic HCOOH or glycine molecule. This participation leads

Table III. Effect of Basis Set on Calculated Transition State Energy[a]

	ΔU^*_1 of transition state T1
NH_3–HCOOH Reaction	
HF/6-31G//HF/STO-3G	42.2
HF/6-31G//HF/6-31G	46.9
MP4(SDQ)/6-31G**//HF/6-31G**	41.8
Mg^{2+}-Catalyzed NH_3–Glycine Reaction	
HF/6-31G//HF/STO-3G	3.7
HF/6-31G//HF/6-31G	8.5

[a] Energies are in kcal/mol; see Table II for notations used in this table.

to nonplanar six-membered cyclic transition states and net decreases in the free energies of activation of about 10 kcal/mol despite the unfavorable decreases in entropies of activation. Thus in the Mg^{2+}-catalyzed NH_3–glycine reaction described here, a further reduction of free energy of activation is quite possible by direct involvement of a protic solvent. However, based on previous results, it is unlikely that the added catalytic effect of a solute molecule would alter the manner or relative effect of the Mg^{2+} cation on reactant, transition states, or intermediate.

In the present study, the relative energies were calculated using geometries optimized by STO-3G basis set. Table III summarizes the relative internal energy ΔU^*_1 of the first transition state of the two-step reaction using geometries optimized by more flexible basis sets for the NH_3–HCOOH and Mg^{2+}-catalyzed NH_3–glycine reactions. The ΔU^*_1 values calculated at HF/6-31G level were lower by only 4.7 and 4.8 kcal/mol in the former and the latter reactions, respectively, when the STO-3G optimized geometry was used. Further, in the former reaction the geometries were optimized using the 6-31G** basis set[12] which includes a d-type polarization function on heavy atoms and a p-type polarization function on hydrogen atoms; with these geometries ΔU^*_1 was calculated using Möller–Plesset perturbation at the fourth order.[13] In consequence of the opposite effects of electron correlation and polarization, a result obtained at the HF/6-31G level is very similar to that obtained at the MP4/6-31G** level. Cancellation of these two effects was also observed in the previous studies of NH_3-catalyzed[3b] and uncatalyzed[3a] NH_3–HCOOH reactions as is seen in Table II. Thus, based on the results given in Table II and III, the relative energetics between Mg^{2+}-catalyzed and uncatalyzed reactions are not expected to change significantly, when the higher level of theory including effects of electron correlation and polarization is used.

In the present study, Mg^{2+} cation is coordinated by only two atoms, and the effect of further coordination by solvent molecules should be considered. Thus, theoretical study of the system NH_3 + $HH_2CH_2COOH{\cdot}Mg^{2+}{\cdot}2H_2O$ has been initiated, where two water molecules are coordinated to the Mg^{2+} cation. The effectiveness of Mg^{2+} as a catalyst when its positive charge is reduced by further coordination is of particular interest.

Conclusion

The two-step and concerted reaction mechanisms of Mg^{2+}-catalyzed amide bond formation between NH_3 and glycine molecules have been characterized. The major conclusions from this study are the following.

(1) As was found in the uncatalyzed amide bond formation, the Mg^{2+}-catalyzed reaction involves simultaneous nucleophilic attack of the amine on the carbonyl carbon atom and transfer of a hydrogen atom to an oxygen atom leading to planar, four-membered ring transition states. Further, since for each transition state the Mg^{2+} cation makes a nonplanar, five-membered chelate ring by bonding to the carbonyl oxygen and amine nitrogen atoms, all the transition states found here have a bicyclic structure.

(2) For all the transition states in the Mg^{2+}-catalyzed reaction, the free energies of activation are substantially lower than those found in the uncatalyzed reaction. The major factors causing this stabilization are the neutralization of the developing negative charge on the carbonyl oxygen atom by the Mg^{2+} cation and the ability of the Mg^{2+} cation to form conformationally flexible nonplanar, five-membered chelate ring structures.

(3) A tetrahedral intermediate found in the Mg^{2+}-catalyzed reaction is structurally similar to that found in the uncatalyzed reaction, except that the formation of a nonplanar, five-membered chelate ring by the Mg^{2+} occurs. This chelation substantially stabilizes the intermediate and is consistent with the spectrophotometrical detection of an intermediate reported in Co^{3+}-catalyzed peptide bond formation.

(4) The two-step and concerted reaction mechanisms catalyzed by Mg^{2+} are equally competitive.

Acknowledgment. Support from NASA-Ames Cooperative Agreement NCC2-196 with The Rockefeller University is acknowledged. We are indebted to Drs. D. Spangler and D. DeFrees for helpful discussions. We also thank Miss W. Davis for preparation of the manuscript.

Registry No. Mg, 7439-95-4; NH_3, 7664-41-7; $NH_2CH_2CONH_2$, 598-41-4; glycine, 56-40-6.

(12) Hariharan, P. C.; Pople, J. A. *Theor. Chim Acta* **1973**, *28*, 213.
(13) (a) Möller, C.; Plesset, J. *Phys. Rev.* **1934**, *46*, 618. (b) Binkley, J. S.; Pople, J. A. *Int. J. Quantum Chem.* **1975**, *9*, 229. (c) Pople, J. A.; Binkley, J. S.; Seeger, R. *Int. J. Quantum Chem. Symp.* **1976**, *10*, 1. (d) Pople, J. A.; Krishnan, R.; Schlegel, H. B.; Binkley, J. S. *Int. J. Quantum Chem.* **1978**, *14*, 545.